Starlink-26 satellite re-entry determination

A.I. Nazarenko. April 2021
anazarenko32@mail.ru, satmotion.ru

1. IADC 2021 test campaign

The current test object is the starlink-26 satellite (identified via cospar id 2019-029f or norad id 44240). it was launched from Kennedy space center (etr, united states) on 2019-05-24 02:24utc into an orbit with an approximate perigee height of 442 km and an approximate apogee height of 445 km, with an inclination of 53 deg. the satellite has a flat box shape of dimensions 3.7m length, 1.5m width and 0.2m height, with 1 solar panel deployed which could be perpendicular or parallel to the satellite body, with 2.8m length and 8.1m width, with a dry mass of about 227 kg.

Its orbit on 22-march-2021 had approximately a perigee and apogee height of 317 km and 320 km with a 53 deg inclination. with this, and depending on the atmospheric model used, a re-entry between 2 and 11 April 2021 is expected.

2. Technique of re-entry determination

To solve the problem in question, the author used the methodology of the optimal filtration of measurements, which is detailed in the articles [1], [2] and book [3]…As a result of analysis, the comparative relationships were established between the errors of state vector estimates with using the considered methods (approaches). The analysis results are presented. It is seen from this data that, for any level of disturbances, *thebest accuracy is achieved with applying the optimal measurement filtering technique*.The expediency of LST application *without* or *with* state vectorextension depends on the level of disturbances. There existssome level of small disturbances, at which it is more expedient toapply LST without state vector extension. However, even in thiscase the errors are greater, than in the case of using the optimalfiltration of measurements (the nonparametric approach).

3. Results. April 05

As the initial data, the TLE from site of space-track.org [4] are used (see Table 1).

Table 1. Initial TLE values

1 44240U 19029F 21086.57536359 +.00658016 +17910-3 +22060-2 0 09994
2 44240 052.9912 233.1619 0010488 317.3866 042.6344 15.89484802103022
1 44240U 19029F 21086.70110831 +.00684801 +19443-3 +22751-2 0 09993
2 44240 052.9915 232.5214 0010687 317.9347 042.0856 15.89659893103048
1 44240U 19029F 21087.39245847 +.00634550 +16883-3 +20108-2 0 09990
2 44240 052.9915 228.9956 0011245 322.1213 037.9020 15.90577205103933

1 44240U 19029F   21087.51811190 +.00795589 +26820-3 +24883-2 0 09990
2 44240 052.9909 228.3554 0011376 323.0255 036.9984 15.90835013103173
1 44240U 19029F   21087.70656876 +.00732354 +22679-3 +22620-2 0 09995
2 44240 052.9904 227.3925 0011445 323.8498 036.1752 15.91073170103986
1 44240U 19029F   21088.71122468 .00643739 17732-3 18710-2 0 9999
2 44240 52.9893 222.2555 0012084 327.8085 32.2201 15.92230120103361
1 44240U 19029F   21088.71122468 .00643739 17732-3 18710-2 0 9999
2 44240 52.9893 222.2555 0012084 327.8085 32.2201 15.92230120104148
1 44240U 19029F   21089.08778468 .00573158 14175-3 16308-2 0 9993
2 44240 52.9892 220.3284 0012418 329.6681 30.3625 15.92631610104203
1 44240U 19029F   21089.52696459 .00632160 17313-3 17446-2 0 9991
2 44240 52.9891 218.0785 0012648 331.7267 28.3071 15.93203176104273
1 44240U 19029F   21089.65241761 .00600187 15650-3 16441-2 0 9997
2 44240 52.9896 217.4362 0012753 332.0488 27.9851 15.93342156103517
1 44240U 19029F   21089.65241761 .00600187 15650-3 16441-2 0 9997
2 44240 52.9896 217.4362 0012753 332.0488 27.9851 15.93342156104293
1 44240U 19029F   21089.65241769 .00637467 17638-3 17449-2 0 9993
2 44240 52.9896 217.4362 0012760 332.1903 27.8439 15.93355220104291
1 44240U 19029F   21090.34219195 .00613150 16500-3 16050-2 0 9996
2 44240 52.9893 213.8991 0013137 335.0419 24.9970 15.94186127103622
1 44240U 19029F   21090.71826153 .00736902 24110-3 18690-2 0 9994
2 44240 52.9892 211.9703 0013352 336.8007 23.2415 15.94771129104463
1 44240U 19029F   21091.21945717 .00870280 34590-3 21053-2 0 9996
2 44240 52.9882 209.3962 0013360 337.9293 22.1157 15.95658818103761
1 44240U 19029F   21091.21945717 .00870280 34590-3 21053-2 0 9996
2 44240 52.9882 209.3962 0013360 337.9293 22.1157 15.95658818104548
1 44240U 19029F   21091.53254863 .01068272 54577-3 24943-2 0 9995
2 44240 52.9877 207.7856 0013358 338.3314 21.7147 15.96346882104597
1 44240U 19029F   21091.84551697 .00964886 44029-3 21769-2 0 9993
2 44240 52.9863 206.1724 0013322 339.7088 20.3408 15.96948676103866
1 44240U 19029F   21091.84551697 .00964886 44029-3 21769-2 0 9993
2 44240 52.9863 206.1724 0013322 339.7088 20.3408 15.96948676104643
1 44240U 19029F   21091.90809634 .00971684 44805-3 21769-2 0 9993
2 44240 52.9882 205.8497 0012734 335.6989 24.3778 15.97092220104659
1 44240U 19029F   21092.53358959 .01112864 61823-3 23158-2 0 9993
2 44240 52.9908 202.6207 0012529 339.7636 20.2858 15.98456501104750
1 44240U 19029F   21092.59611014 .01053007 54685-3 21774-2 0 9996
2 44240 52.9849 202.2991 0013693 341.8068 18.1959 15.98522105104769
1 44240U 19029F   21092.78366116 .01011345 50284-3 20483-2 0 9993
2 44240 52.9837 201.3330 0013833 342.4855 17.5694 15.98875739104785
1 44240U 19029F   21092.78366116 .01091706 59675-3 22077-2 0 9996
2 44240 52.9863 201.3247 0013280 338.0476 22.0448 15.98938493104793

1 44240U 19029F 21093.15857712 .01137880 66431-3 21981-2 0 9990
2 44240 52.9861 199.3894 0012546 337.4648 22.5706 15.99776745104853
1 44240U 19029F 21093.42998043 .00879608 37798-3 16634-2 0 9996
2 44240 52.9835 197.9885 0012510 344.8443 139.1129 16.00087157104897
1 44240U 19029F 21093.47094370 .01105800 62838-3 20691-2 0 9999
2 44240 52.9835 197.7764 0012511 345.4631 14.6486 16.00324543104906
1 44240U 19029F 21093.53338277 .01097756 61926-3 20408-2 0 9996
2 44240 52.9870 197.4579 0012503 344.8956 15.1238 16.00435009104912
1 44240U 19029F 21093.84557786 .01058408 57589-3 18966-2 0 9995
2 44240 52.9819 195.8316 0014533 345.3301 14.7247 16.01002287104960
1 44240U 19029F 21094.15762666 .00942788 44913-3 16422-2 0 9999
2 44240 52.9796 194.2174 0014250 347.9432 11.8537 16.01467862105019
1 44240U 19029F 21094.48384264 .01081254 61564-3 18195-2 0 9992
2 44240 52.9828 192.5192 0013526 348.2463 93.7748 16.02111446105062
1 44240U 19029F 21094.84383545 .01024740 55245-3 16520-2 0 9999
2 44240 52.9843 190.6503 0013119 348.3694 11.6645 16.02831323105124

The results of the optimal measurement filtration technique to determine the current drag parameter (ballistic factor) are presented in Figure 1.

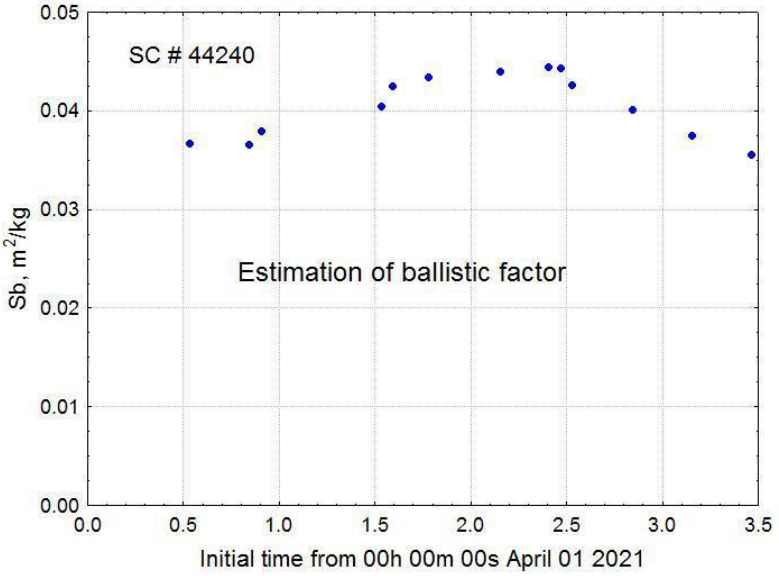

Figure 1. Estimation of ballistic factor (Sb)

Here, the deviations of the current ratings of the Sb from the average value do not exceed ±11%. Table 2 provides estimates of the time of entry into the dense atmosphere (reaching an altitude of 80 km).

.Таблица 2. Determination of reentry time

Time from April 01		Date	hh	mm
Initial	Reentry			
0.219	9.456	April 10	10	56
3.47	8.641	April 09	15	22

Here, the differences in entry time estimates correspond to variations of Sb values.

6. Results. April 06

The results of the optimal measurement filtration technique to determine the current drag parameter (ballistic factor) are presented in Figure 2.

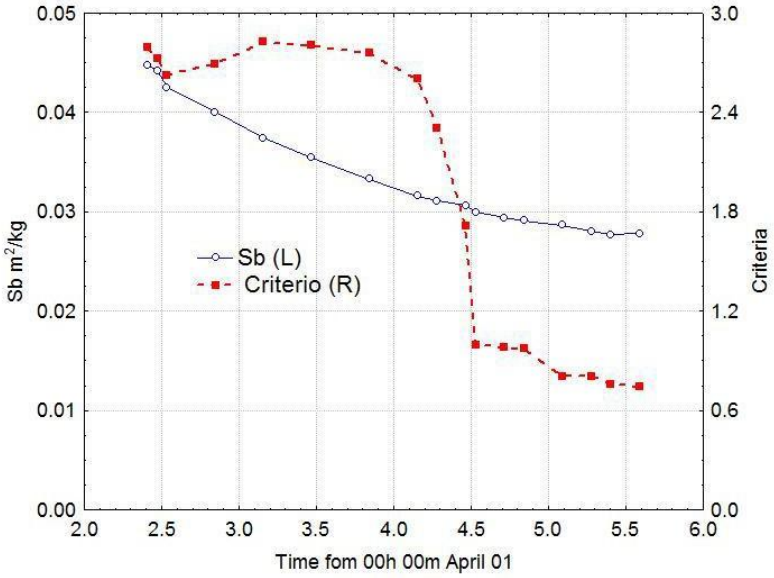

Figure 2. Estimation of ballistic factor (Sb) and minimizing criteria

These data show that ballistic coefficient estimates are stabilizing. The proximity of the minimizable criteria to 1 indicates that the constructed orbit fits well into the measurements.Table 3 provides all estimates of the time of entry into the dense atmosphere (reaching an altitude of 80 km).

Таблица 3. Determination of reentry time

Time from April 01		Date	hh	mm
Initial	Reentry			
0.219	9.456	April 10	10	56
3.47	8.641	April 09	15	22
4.841	9.750	April 10	17	59
5.090	8.820	April 10	19	41
5.401	9.941	April 10	22	35
5.588	9.883	April 10	**21**	**11**

The data of the last two lines show the stabilization of estimates of the re-entry time. This is a consequence of the stabilization of Sb's estimates.

Figure 3 shows the Earth map and a calculated route of the satellite's movement at re-entry. The red color highlights the possible scattering of the entry point into the dense layers of the atmosphere.

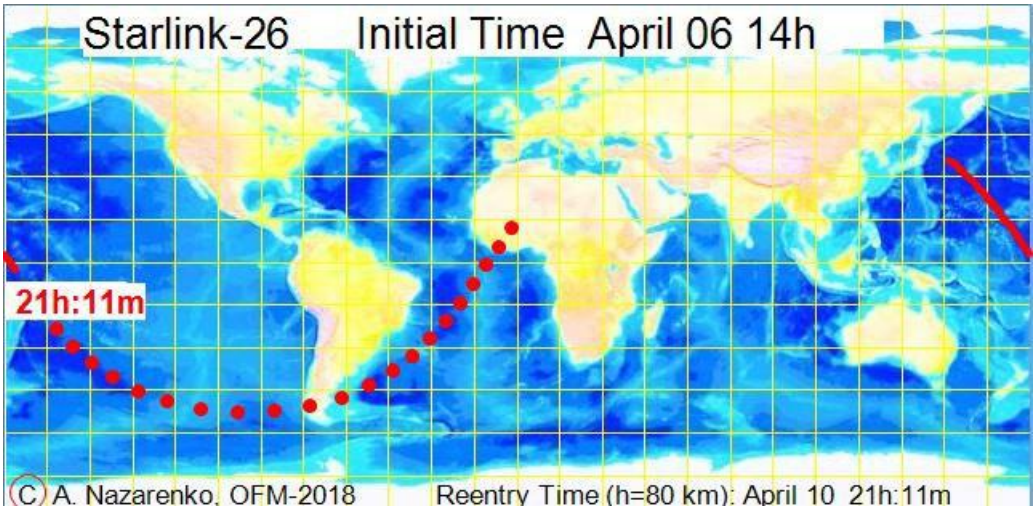

Figure 3. Calculated re-entry route

7. Results. April 07

The results of the optimal measurement filtration technique to determine the current drag parameter (ballistic factor) are presented in Figure 4.

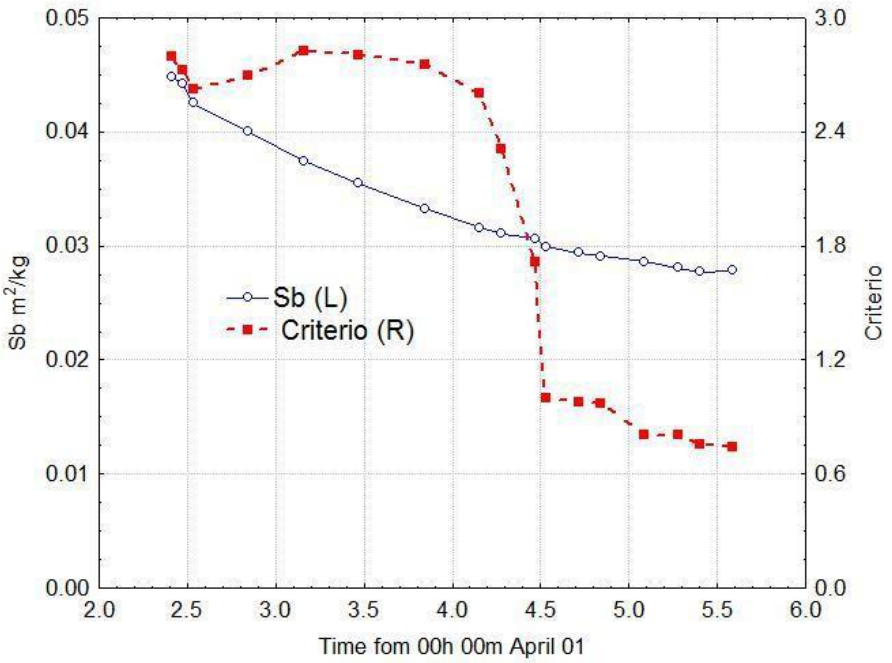

Figure 4. Estimation of ballistic factor (Sb) and minimizing criterio

These data show that ballistic coefficient estimates are stabilizing. The proximity of the minimizable criteria to 1 indicates that the constructed orbit fits well into the measurements. Table 4 provides all estimates of the time of entry into the dense atmosphere (reaching an altitude of 80 km).

Таблица 4. Determination of **re-entry time**

Time from April 01		Date	hh	mm
Initial	Reentry			
0.219	9.456	April 10	10	56
3.47	8.641	April 09	15	22

4.841	9.750	April 10	17	59
5.090	8.820	April 10	19	41
5.401	9.941	April 10	22	35
5.588	9.883	April 10	21	11
5.712	9.799	April 10	19	09
6.209	9.736	April 10	**17**	**39**

The data of the last two lines show the the approach of the re-entry time by 1.5 hours (2% of the life time). This is the result of a small increase in the Sb value.

Figure 5 shows the Earth map and the calculated route of the satellite's movement at re-entry. The red color highlights the possible scattering of the entry point into the dense layers of the atmosphere.

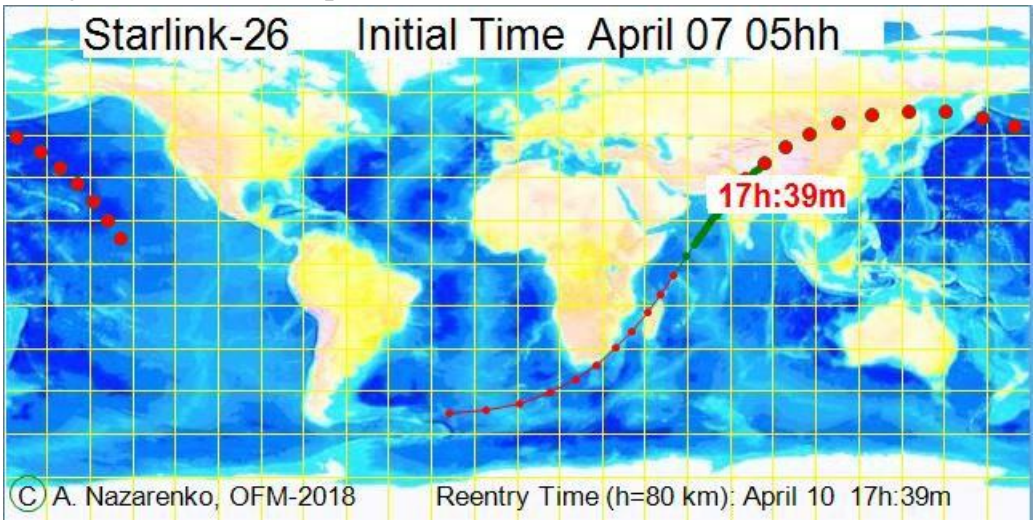

Figure 5. Calculated re-entry route

8. Results. April 08

The results of the optimal measurement filtration technique to determine the current drag parameter (ballistic factor) are presented in Figure 6.

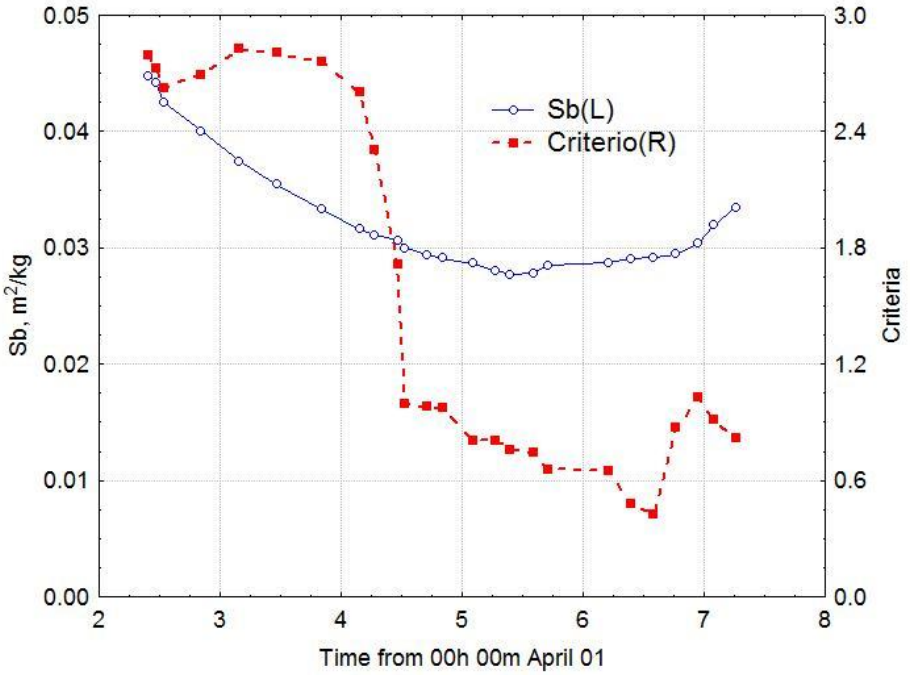

Figure 6. Estimation of ballistic factor (Sb) and minimizing criteria

From these data you can see the growth of the satellite's drag over the last 24 hours. Sb's valuea increased by 22%. This is a very significant increase. That is due to the impact of a geomagnetic storm that occurred on 7 April (see figure 7)

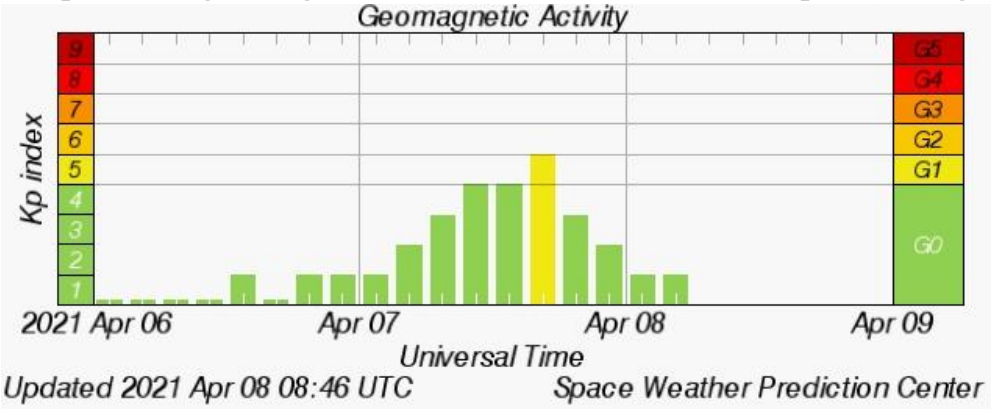

Figure 7. Geomanite activity. Kp index values

In the previous forecast of the re-entry time, the impact of a possible geomagnetic storm was not taken into account. Therefore, it should be expected that the increase in the Sb value will lead to a significant diminution of the estimated re-entry time (≈ 20% of the life time).

Table 4 provides all estimates of the time of entry into the dense atmosphere (reaching an altitude of 80 km).

Таблица 4. Determination of **re-entry time**

Time from April 01		Date	hh	Mm
Initial	Reentry			
0.219	9.456	April 10	10	56
3.47	8.641	April 09	15	22
4.841	9.750	April 10	17	59
5.090	8.820	April 10	19	41
5.401	9.941	April 10	22	35
5.588	9.883	April 10	21	11
5.712	9.799	April 10	19	09
6.209	9.736	April 10	**17**	**39**
7.264	9.062	April 10	**01**	**29**

The data of the last two lines show the the diminution of the re-entry time by 16 hours (21% of the life time). This is the result of increase in the Sb value.

Figure 8 shows the Earth map and the calculated route of the satellite's movement at re-entry. The red color highlights the possible scattering of the entry point into the dense layers of the atmosphere.

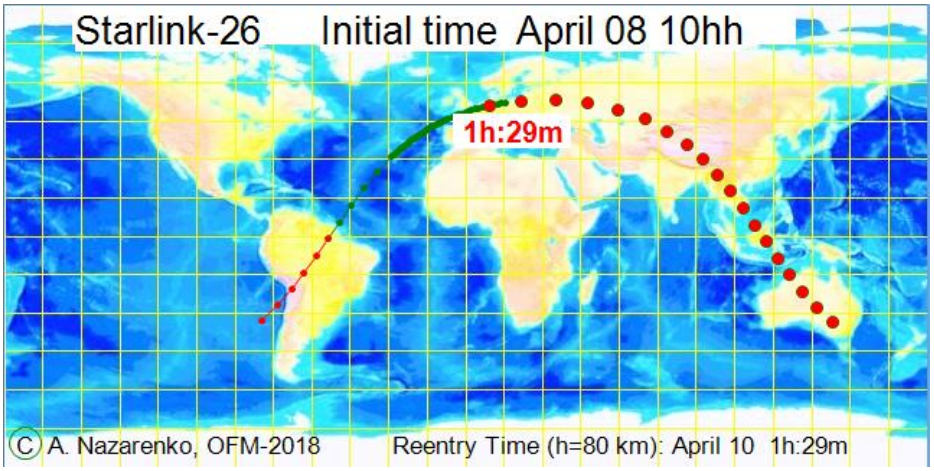

Figure 8. Calculated re-entry route

From these data it is clear that the combustion of the satellite during re-entry can be observed from the territory of Russia.

9. Results. April 09

The results of the optimal measurement filtration technique to determine the current drag parameter (ballistic factor) are presented in Figure 9.

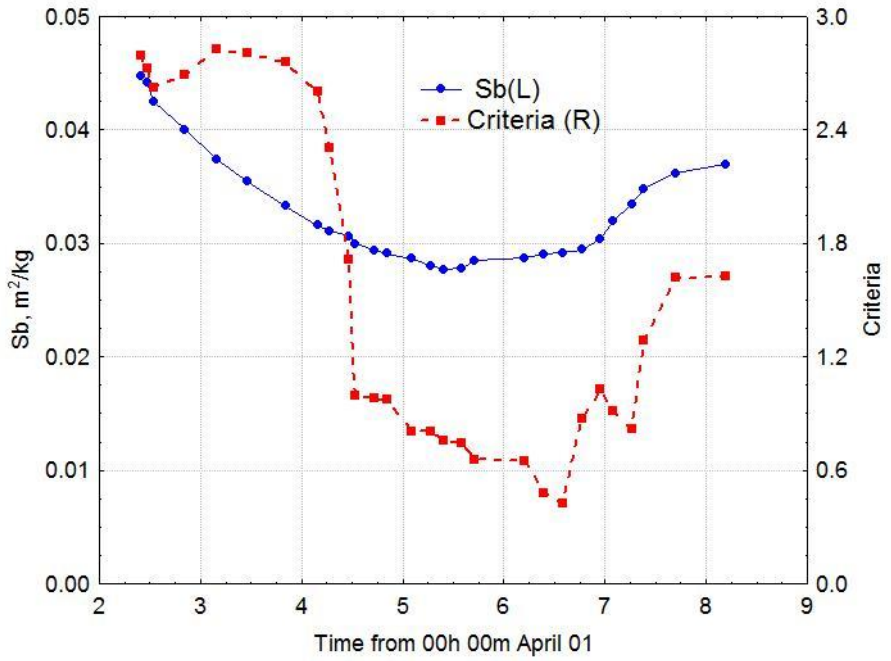

Figure 9. Estimation of ballistic factor (Sb) and minimizing criteria

It is clear from these data that the Sb estimates have stabilized.

Table 5 provides all estimates of the time of entry into the dense atmosphere (reaching an altitude of 80 km).

Таблица 5. Determination of **re-entry time**

Time from April 01		Date	hh	mm
Initial	Reentry			
0.219	9.456	April 10	10	56
3.47	8.641	April 09	15	22
4.841	9.750	April 10	17	59
5.090	8.820	April 10	19	41
5.401	9.941	April 10	22	35

5.588	9.883	April 10	21	11
5.712	9.799	April 10	19	09
6.209	9.736	April 10	**17**	**39**
7.264	9.062	April 10	**01**	**29**
7.388	9.024	April 10	**00**	**35**
7.697	9.045	April 10	**01**	**05**
8.191	9.188	April 10	**04**	**31**

The data of the last two lines show the increase of the re-entry time by 3 hours 26 minutes (15% of the life time). This is the result of weakening of drag in the atmosphere after the geomagnetic storm.

Figure 10 shows the Earth map and the calculated route of the satellite's movement at re-entry. The red color highlights the possible scattering of the entry point into the dense layers of the atmosphere.

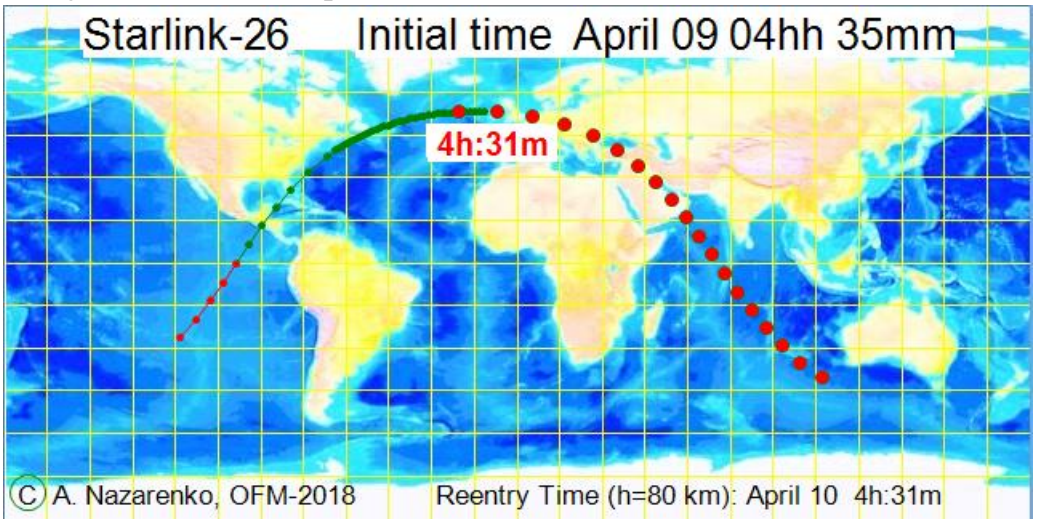

Figure 10. Calculated re-entry route

From these data it is clear that the combustion of the satellite during re-entry can be observed from the territory of Europe and Russia.

Reference.

1. Nazarenko AI. Comparison of Various Methods for Orbital Measurements Processing. International Journal of Aeronautical Science & Aerospace Research (IJASAR 2470-4415-06-30), 2019.
2. Nazarenko AI. How can we increase the accuracy of determination of spacecraft's lifetime? ActaAstronautica; 2015 Nov 1. 116 :229-36.
3. Назаренко АИ. Задачи стохастической космидинамики. Математиченские методы и алгоритмы решения. М. ЛЕНАНД, 20182-352 с.
4. Spacetrack.org

April 09. 11^{hh}